New types of dose distributions for vertical sidewall minimizing total dose in 3-D electron-beam proximity effect correction of nanoscale features

Qing Dai and Soo-Young Lee[a)]
Department of Electrical and Computer Engineering, Auburn University, Auburn, Alabama 36849

Sang-Hee Lee, Byung-Gook Kim, and Han-Ku Cho
Samsung Electronics, Photomask Division, 16 Banwol-Dong, Hwasung, Kyunggi-Do, Korea

(Received 29 June 2012; accepted 30 October 2012; published 26 November 2012)

The spatial dose distribution across a feature, derived by a conventional 2-D proximity effect correction scheme, is a "V-shape," i.e., higher dose closer to edges. With such a dose distribution, it is extremely difficult to realize a vertical sidewall in the resist profile for nanoscale features while reducing the critical dimension (CD) error. In this paper, it is shown that, in order to achieve a vertical sidewall of nanoscale feature with the minimum total dose, a dose distribution of a shape other than the V-shape must be used. This is due to the fact that the lateral development of resist becomes comparable to the vertical development for nanoscale features and the exposure varies along the depth dimension with high and low contrasts at the top and bottom layers of resist, respectively. Based on these characteristics, new types of dose distributions, i.e., "M-shape" and "A-shape," have been derived to achieve a target resist profile of a vertical sidewall while minimizing the total dose. The simulation results show that the new dose distribution types lead to a more vertical sidewall, a smaller CD error, and a lower total dose. © *2012 American Vacuum Society*. [http://dx.doi.org/10.1116/1.4767446]

I. INTRODUCTION

The proximity effect due to electron scattering in the resist limits the minimum feature size and the maximum circuit density that can be fabricated by the electron-beam (e-beam) lithographic process. The importance of the proximity effect correction (PEC) has been well recognized and extensively investigated, and various effective schemes were developed.[1–9] A typical two-dimensional (2-D) PEC scheme does not take into account the variation of exposure (e-beam energy deposited) along the resist depth dimension, and deconvolves the 2-D target exposure distribution by the point spread function (*PSF*) to derive a correction result, i.e., the required dose (e-beam energy given) distribution. For the most common sidewall shape, i.e., the vertical sidewall, a typical 2-D target exposure distribution is constant within and zero outside a feature. In this case, the required dose distribution obtained by the deconvolution is a "V-shape," i.e., the dose is highest at the edge and gradually decreases toward the center of the feature. However, our earlier studies have shown that such a 2-D PEC does not lead to realistic results, especially for nanoscale features, and therefore, true three-dimensional (3-D) PEC is needed.[10–13] In 3-D PEC, the resist profile estimated through a simulation of resist development was employed, instead of the exposure distribution, in order to obtain more realistic results. Moreover, it has been demonstrated that in order to minimize any deviation from a target resist profile, a 3-D PEC scheme must check the estimated resist profile during the dose optimization procedure.[11,13] One practical issue of such an approach to 3-D PEC is that a time-consuming resist-development simulation needs to be carried out in each iteration of the dose optimization. Also, it is shown that the "V-shape" dose distribution is not optimal for realizing a vertical sidewall in the resist profile, especially when the total dose is to be minimized. Note that a higher total dose worsens the charging effect and lengthens the exposing time.

In this study, an efficient optimization scheme which derives the dose distribution required to achieve a target 3-D resist profile has been developed. For estimating the resist profile during the optimization, a fast path-based method is employed instead of a time-consuming cell-based method. The systematic dose updating procedure coupled with the fast resist development simulation makes the dose optimization scheme fast and effective. The most noteworthy result from this study is that in order to achieve a vertical sidewall of nanoscale feature with the minimum total dose, one has to employ a dose distribution different from the conventional "V-shape." Based on our 3-D model and PEC, new dose distributions with an "M-shape" and "A-shape" have been derived for achieving the target resist profile of a vertical sidewall while minimizing the total dose. Through an extensive simulation, these new dose distributions are compared with other distributions, uniform and "V-shape," in terms of deviation from the target resist profile of a vertical sidewall.

The rest of the paper is organized as follows. The simulation of exposure and development are briefly described in Sec. II. Details of the conventional and proposed dose distribution types are presented in Sec. III. The proposed dose optimization scheme is described in Sec. IV. Simulation results are discussed in Sec. V, followed by a summary in Sec. VI.

II. SIMULATION OF EXPOSURE AND DEVELOPMENT

A. Exposure model

In a typical substrate system employed in this study, a resist layer with an initial thickness of H is on top of the

a)Electronic mail: leesooy@eng.auburn.edu

 2166-2746/2012/30(6)/06F307/11/$30.00 © 2012 American Vacuum Society

Downloaded 10 Dec 2012 to 131.204.21.179. Redistribution subject to AVS license or copyright; see http://avspublications.org/jvstb/about/rights_and_permissions

substrate, as illustrated in Fig. 1(a), where the X-Y plane corresponds to the top surface of resist and the resist depth is along the Z-dimension. The 3-D *PSF* is denoted by *psf*(x, y, z), which describes the exposure distribution in the resist when a point on the X-Y plane is exposed. Let $d(x, y, 0)$ represent the e-beam dose given to the point $(x, y, 0)$ on the surface of the resist for writing a circuit feature or pattern [refer to Fig. 1(a)]. For example, in the case of a uniform dose distribution,

$$d(x,y,0) = \begin{cases} D & \text{if } (x,y,0) \text{ is within a feature} \\ 0 & \text{otherwise,} \end{cases} \quad (1)$$

where D is a constant dose.

Let us denote the exposure at the point (x, y, z) in the resist by $e(x, y, z)$. Then, the 3-D spatial distribution of exposure can be expressed by the following convolution:

$$e(x,y,z) = \int\int d(x-x', y-y', 0) psf(x', y', z) dx' dy'. \quad (2)$$

From Eq. (2), it can be seen that the exposure distribution at a certain depth z_0 can be computed by the 2-D convolution between $d(x, y, 0)$ and $psf(x, y, z_0)$ in the corresponding plane $z = z_0$, i.e., $e(x, y, z)$ may be estimated layer by layer. Note that the *PSF*, *psf*(x, y, z), reflects all the phenomena affecting energy deposition including the e-beam blur. The goal of PEC is to determine $d(x, y, 0)$ such that a target pattern is successfully transferred onto the resist layer.

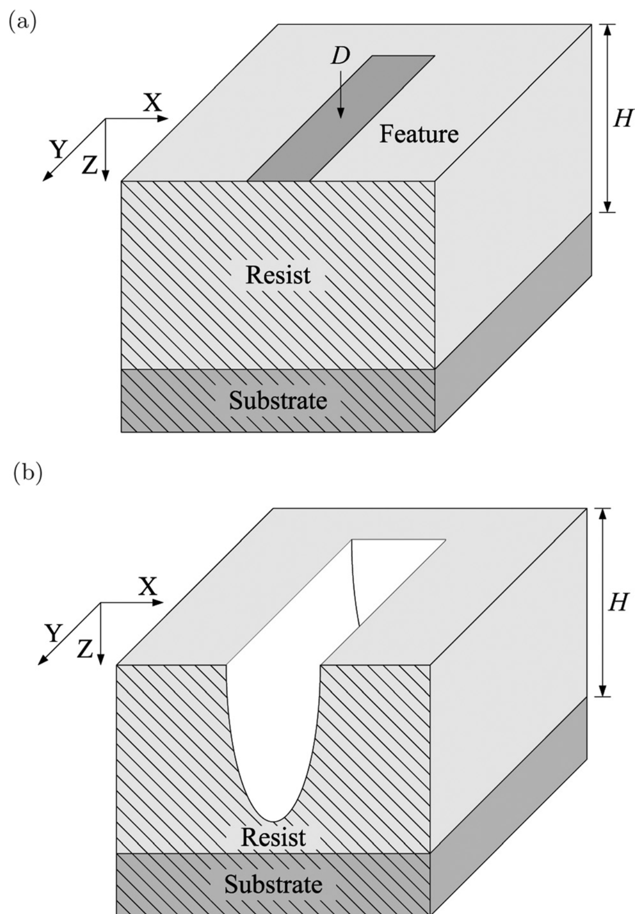

FIG. 1. Illustration of (a) the substrate system where H is the initial thickness of the resist and (b) the final remaining resist profile after the development process.

B. Development method

Although the 3-D exposure model provides the complete information on how electron energy is distributed in the resist, it does not directly depict the remaining resist profile after development, as illustrated in Fig. 1(b). Therefore, it is necessary to also take the resist development process into account in order to obtain a realistic correction result. However, a cell-based resist development simulation such as the "cell removal method," e.g., PEACE,[14] is too time-consuming to be employed in an iterative correction procedure. In the cell removal method, the resist layer is partitioned into cubic cells, and the resist development process is traced on a cell-by-cell basis.

Instead of employing the time-consuming cell-based method, a fast path-based simulation method has been developed in order to be employed in our 3-D PEC. In the path-based method, the developing process is traced along vertical (to depict vertical development) and lateral (to depict lateral development) paths in the resist.

The developing rate $r(x, y, z)$ along each path is calculated from its corresponding exposure $e(x, y, z)$ through a nonlinear exposure-to-rate conversion formula, which is obtained experimentally. A long line with width of 100 nm is exposed with various dose levels. After resist development, the center depth is measured in the cross-section of remaining resist profile obtained for each dose level. Note that the resist is developed only vertically at the center of line when the dose distribution within the line is uniform. The center depth is also obtained for each dose level through simulation based on our 3-D exposure model. By comparing the two sets of depth measurements obtained experimentally and via simulation, the following conversion formula has been derived:

$$\begin{aligned} r(x,y,z) &= F[e(x,y,z)] \\ &= 3700 \cdot e^{-\left(\frac{e(x,y,z)-1.0e11}{5.6e10}\right)^2} - 80 \cdot e^{-\left(\frac{e(x,y,z)-9.0e9}{9.0e9}\right)^2} - 123, \end{aligned} \quad (3)$$

where $r(x, y, z)$ is in nm/minute and $e(x, y, z)$ in $\mathrm{eV}/\mu\mathrm{m}^2$.

Based on the developing rate distribution and a specified developing time, the resist development along each path (how far the developer goes) can be determined to obtain the final remaining resist profile. Details of the path-based method will be presented in a separate paper.

III. DOSE DISTRIBUTION TYPES

In this paper, only a single feature of a line is considered for simplicity. Suppose that a target written feature is specified by the corresponding resist profile (e.g., line widths at the top, middle, and bottom layers) in 3-D PEC. In our simulation model, the line is sufficiently long in the Y-dimension

Downloaded 10 Dec 2012 to 131.204.21.179. Redistribution subject to AVS license or copyright; see http://avspublications.org/jvstb/about/rights_and_permissions

so that the dimensional variation along the Y-dimension may be ignored. In this case, one only needs to consider the cross-section of the resist profile in the X-Z plane [refer to Fig. 1(b)]. During correction, at each location (x, y) in a circuit pattern, the cross-section of the resist profile needs to be examined. Therefore, $e(x, y, z)$ and $r(x, y, z)$ can be replaced by $e(x, z)$ and $r(x, z)$, respectively.

In order to avoid high complexity of the optimization procedure and also have sufficient spatial control of the dose distribution, the line feature is partitioned into five regions along its length dimension and a dose is determined for each region, as shown in Fig. 2.

The main goal of 3-D PEC is to adjust the spatial distribution of the dose in order to minimize the deviation of the resist profile from the target profile. The focus of this study is on investigating the effectiveness of dose-distribution type (shape) in achieving the target resist profile, in particular, a vertical sidewall.

A. Conventional type

The typical shape of a spatial dose distribution across a line feature is highest in the edge regions and gradually decreasing toward the center region (to be referred to as type-V according to its shape). This type of dose distribution is usually obtained by an exposure-based correction where a target 2-D exposure distribution is specified (to be referred to as 2-D exposure correction[12]).

In the 2-D exposure model, the exposure is assumed not to vary along the depth dimension (Z-dimension), i.e., $e(x, z)$ in the cross-section is averaged over $0 \le z \le H$ [refer to Fig. 1(a)], resulting in $e(x)$. Let $h(x)$ represent the depth distribution (i.e., depth at x) in the target resist profile. A target exposure distribution $E_t(x)$ is derived from $h(x)$ by

$$E_t(x) = F^{-1}\left[\frac{h(x)}{T}\right], \tag{4}$$

where T is the developing time.

The exposure $E_t(x)$ can be considered as a threshold for a certain point to be fully developed. Therefore, the objective of this 2-D exposure correction is to control the dose distribution $d(x)$ such that $e(x)$ is as high as the threshold $E_t(x)$ in the exposed area, and as low as possible in the unexposed area, i.e., ideally a rectangular window function with a width of the feature size and a height of $E_t(x)$.

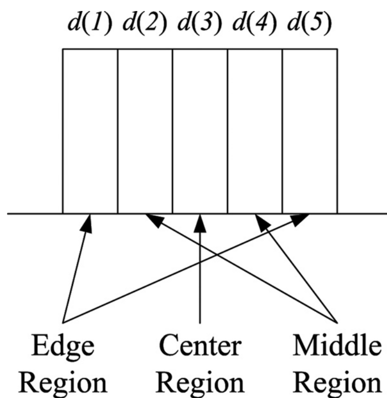

FIG. 2. Region-wise feature partition with a uniform dose distribution.

In this case, the dose distribution $d(x)$ required to achieve this kind of $e(x)$ can be determined through iterations of dose adjustment, or equivalently deconvolution of $e(x)$ with the *PSF*. In general, $d(x)$ derived from deconvolution of a rectangular window function with the *PSF* is of type-V.

The type-V dose distribution seems quite reasonable according to the above analysis. However, when the feature size decreases into nanoscale, it usually results in an undesired 3-D resist profile in terms of feature size and sidewall shape, and requires a relatively higher total dose for full development (refer to Sec. III B for more detail).

This is mainly due to the drawbacks of the 2-D exposure correction. Most importantly, in the 2-D model, the exposure variation along the resist depth dimension is not taken into account, though the resist profile depends on the variation to a great extent. Also, the actual resist profile cannot be derived directly from the exposure distribution, e.g., the resist profile derived from the above-mentioned exposure distribution (a rectangular window function) cannot have a vertical sidewall. The 2-D exposure correction does not consider the resist development process and therefore is likely to end up with an unrealistic result. For example, the lateral development of resist, which significantly affects the resist profile and particularly the sidewall shape of fine features, is not taken into account in the 2-D exposure correction.

B. Proposed types

In order to overcome the drawbacks of the 2-D exposure correction, a resist-profile-based correction was developed along with a 3-D model (to be referred to as 3-D resist profile correction[12]). Unlike the above 2-D exposure correction, this 3-D correction incorporates the estimation of remaining resist profile into the correction procedure and utilizes the resist profile in order to determine the dose distribution based on a 3-D model. The overall correction procedure is similar to that of the 2-D correction. However, the error, which is to be minimized in determining the corrected dose distribution, is computed based on the estimated remaining resist profile rather than the exposure distribution, and is given by

$$Error = \max_j |p(j) - q(j)|, \tag{5}$$

where $p(j)$ and $q(j)$ denote the width distribution of the estimated remaining resist profile and that of the target resist profile, respectively (refer to Fig. 3).

Based on the 3-D resist profile correction, two other types of dose distributions are proposed and analyzed in order to achieve a target resist profile with the minimum total dose. The two new dose distribution types include one with the highest dose in the two middle regions (to be referred to as type-M according to its shape) and the other with the highest dose in the center region and monotonically decreasing

Downloaded 10 Dec 2012 to 131.204.21.179. Redistribution subject to AVS license or copyright; see http://avspublications.org/jvstb/about/rights_and_permissions

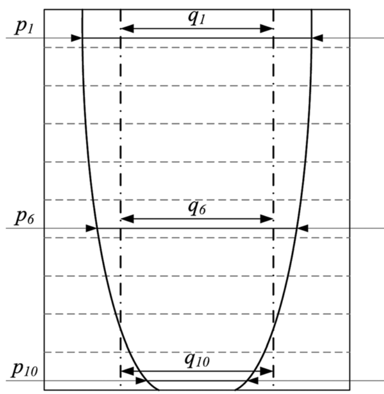

FIG. 3. Cross-section of the resist profile is illustrated for a line feature, where p_j and q_j are the actual and target widths at the j-th layer, respectively, where the resist is modeled by 10 layers.

toward the edge regions (to be referred to as type-A according to its shape).

The effectiveness of the type-M and type-A dose distributions in achieving a vertical sidewall stems from the 3-D distributions of exposure that they result in. In our previous work,[15] it was noticed that the distribution of exposure along the depth dimension behaves quite differently between the exposed area and the unexposed area, as shown in Figs. 4(a) and 4(b). For the exposed area, the exposure usually decreases along the depth dimension, while it changes abruptly to an increasing behavior in the unexposed area.

For a given point x_i, the distribution of its self-exposure [denoted as $e_s(x_i, z)$] decreases along the depth dimension, but the distribution of the sum of exposure contributions from its neighboring points [denoted as $e_o(x_i, z)$] increases along the depth dimension. It is obvious that the overall behavior of exposure distribution for that point, i.e., $e(x_i, z) = e_s(x_i, z) + e_o(x_i, z)$, depends on the dose distribution. If the region which the point belongs to has a relatively lower dose while its neighboring regions have high doses, then $e_o(x_i, z)$ becomes the dominant component and $e(x_i, z)$ tends to increase with z, and vice versa [refer to Figs. 4(c) and 4(d)].

Based on this observation, the resist developing behaviors of different dose types can be analyzed, which are shown in Figs. 5–7 where a thicker arrow corresponds to a higher developing rate. The developing time is given by T, while T_1 and T_2 are two intermediate points in time with $T_1 < T_2 < T$.

For the vertical sidewall shape, take the type-A dose distribution for an example (also refer to Fig. 7). The top layer of resist develops earlier than the bottom layer of resist in the center region. However, the exposure distribution of the edge and middle regions increases in the type-A. As a result, the developing rate of the bottom layer of resist is higher than that of the top layer for the edge and middle regions. Therefore, when the developer reaches the bottom layer of resist and begins to develop laterally from the center region toward the edge regions, it finally catches up with the developing process of the top layer of resist at the boundaries of the feature (the boundaries between the exposed area and the

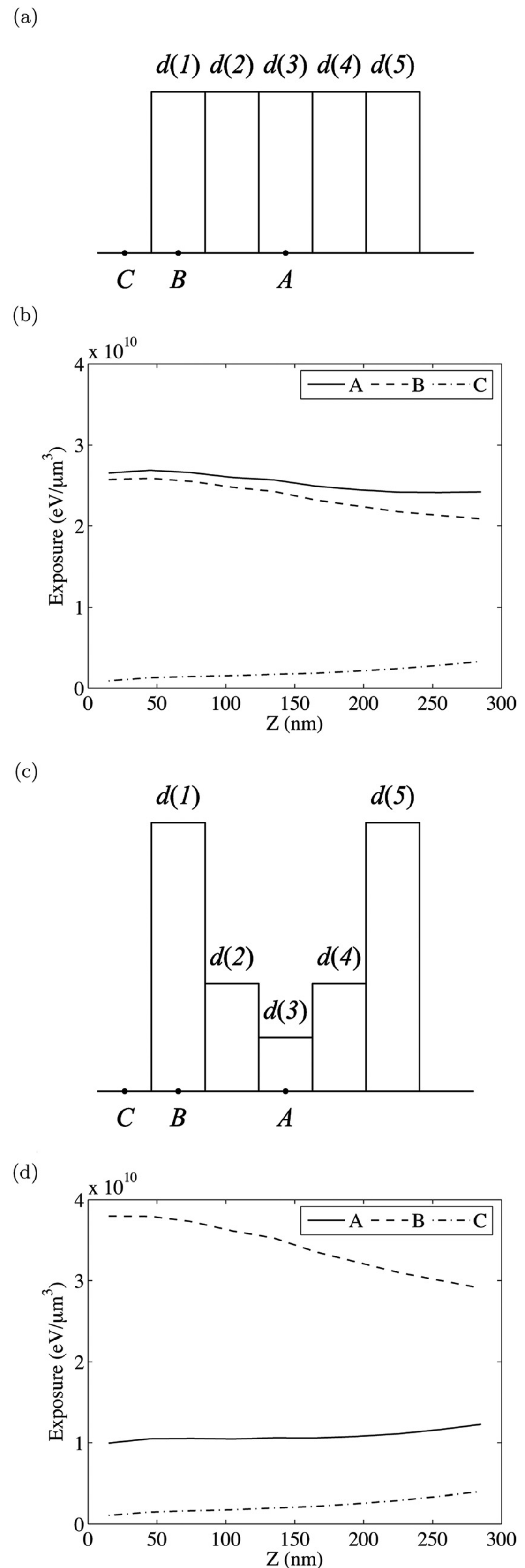

FIG. 4. Comparison of (a) the uniform dose distribution and (b) the corresponding distribution curves of 3-D exposure along the Z-dimension (resist depth), with (c) a nonuniform dose distribution and (d) the corresponding distribution curves of 3-D exposure along the Z-dimension (resist depth) at three points (A, B, and C) on the substrate system of 300 nm PMMA on Si.

Downloaded 10 Dec 2012 to 131.204.21.179. Redistribution subject to AVS license or copyright; see http://avspublications.org/jvstb/about/rights_and_permissions

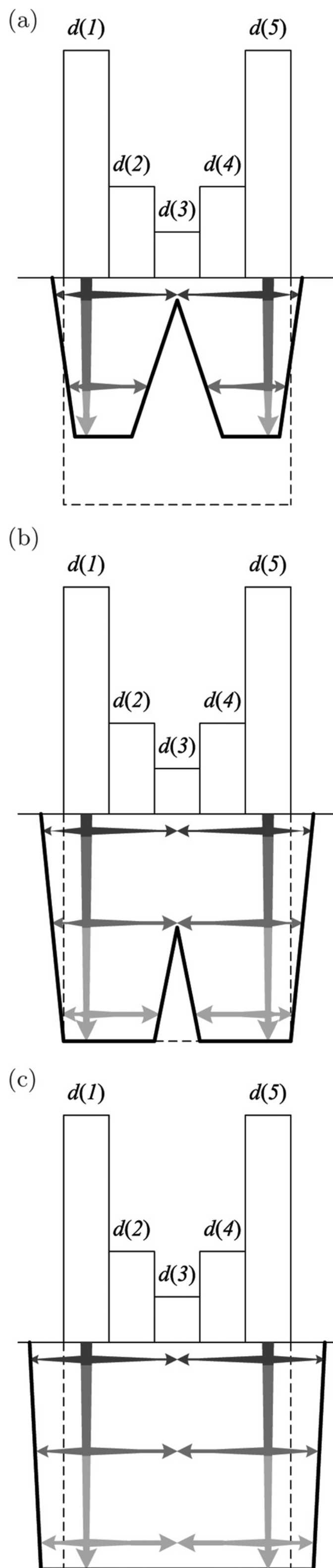

FIG. 5. Resist profile during the development process (a) at time T_1, (b) at time T_2, and (c) at time T for type-V case, where $T_1 < T_2 < T$.

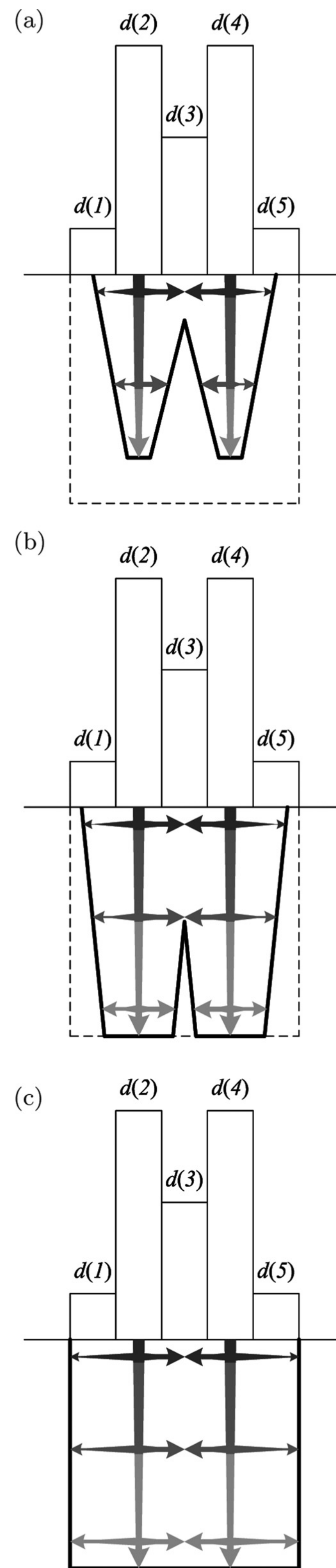

FIG. 6. Resist profile during the development process (a) at time T_1, (b) at time T_2, and (c) at time T for type-M case, where $T_1 < T_2 < T$.

unexposed area) and achieves a vertical sidewall. Note that the exposure distribution in the top layer has a larger contrast over the feature boundaries.

From Fig. 5, it is also seen that the type-V cannot achieve the target vertical sidewall. In the type-V, the top layer of resist always develops earlier than the bottom layer of resist within the edge regions. As a result, the developing process of the bottom layer of resist can never catch up with that of the top layer before reaching the boundaries, thus resulting in an overcut sidewall. This problem may be solved by

Downloaded 10 Dec 2012 to 131.204.21.179. Redistribution subject to AVS license or copyright; see http://avspublications.org/jvstb/about/rights_and_permissions

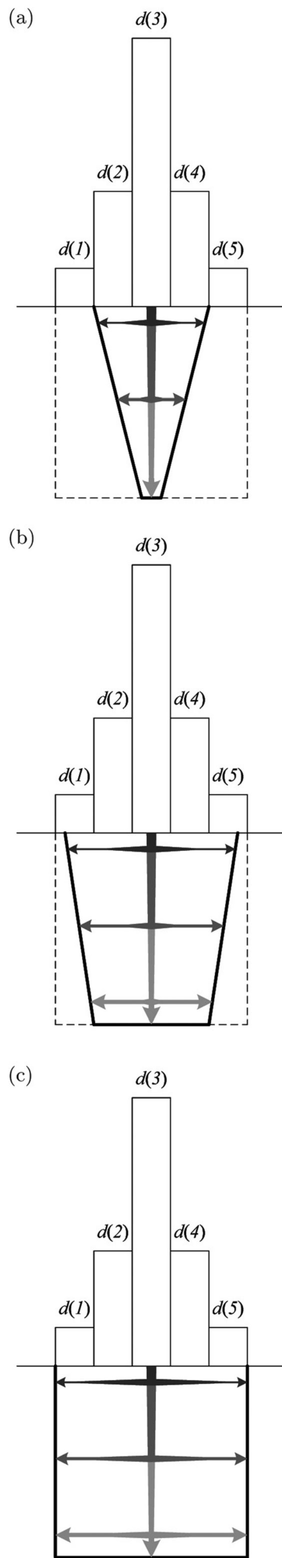

FIG. 7. Resist profile during the development process (a) at time T_1, (b) at time T_2, and (c) at time T for type-A case, where $T_1 < T_2 < T$.

introducing shape correction, i.e., exposing an area smaller than the feature. However, in that way, the type-V becomes an implicit version of the type-M. Another solution is to give a higher total dose for the type-V case to let the bottom layer develop longer, which however requires a higher total dose and tends to make the width of the written feature greater than the target width.

Note that the new finding of type-M and type-A dose distributions would not have been possible without using our 3-D model and PEC.

IV. DOSE OPTIMIZATION SCHEME

An efficient iterative optimization scheme has been developed, which derives the dose distribution of each type and minimizes the deviation from the target resist profile, i.e., vertical sidewall. Each iteration of the optimization scheme consists of three steps: fast exposure computation, path-based resist development process, and type-based dose updating.

In the first step, the three base exposures (region-wise) $(e_i(x,z) \mid i = 1,2,3)$ are precalculated using the 3-D exposure model (refer to Sec. II A). Note that $e_i(x,z)$ is the exposure when a unit dose is given only to the i-th and $(6-i)$-th regions, i.e., $d(i) = 1.0$ and $d(6-i) = 1.0$ while the other regions are not exposed (refer to Fig. 8).

The total exposure $e(x, z)$ can be computed by

$$e(x,z) = \sum_{i=1}^{3} d(i) \cdot e_i(x,z), \tag{6}$$

where $d(i)$ is the actual dose distribution given to the i-th region. The exposure is then converted into developing rate through Eq. (3).

The main goal is to achieve the minimal deviations from the target 3-D resist profile at the top, middle, and bottom layers of the resist. Therefore, in the second step, the simulation of resist development process is employed to generate the resist profile. For this stage, it is not required to run the whole simulation to get a complete resist profile since only the widths at the top, middle, and bottom layers of the resist need to be considered. Therefore, our path-based method (refer to Sec. II B) is further simplified by tracing the developing process along several critical paths required to obtain those desired widths only. Note that the critical paths are not fixed but depend on the specific dose distribution type (refer to Figs. 5–7).

At this point, the width information derived is used for computing width errors. The width errors are defined at the top, middle, and bottom layers of the resist, which is the same as in our previous works (refer to Fig. 3).[11,13] One improvement here is that, besides the outer width error (deviation from the feature boundary), we now also define the inner width error (deviation from the feature centerline), as shown in Fig. 9. These errors are measured for each layer in order to guarantee not only feature size and sidewall shape but also the fully developed condition.

In the third step, the dose of each region is updated based on the current resist profile. Depending on the relationship among the width errors (positive or negative, larger or smaller, etc.), the dose either increases or decreases. The overall dose updating mechanism is common for different

Downloaded 10 Dec 2012 to 131.204.21.179. Redistribution subject to AVS license or copyright; see http://avspublications.org/jvstb/about/rights_and_permissions

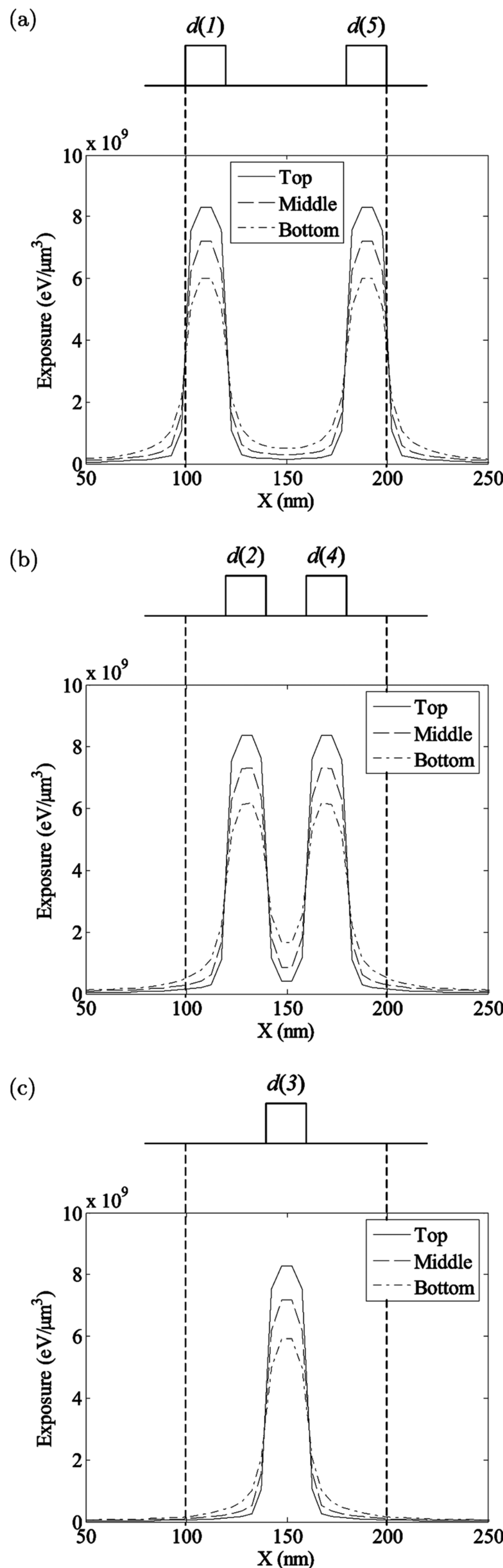

FIG. 8. Exposure distribution of the top, middle and bottom layers of resist when only (a) the two edge regions, (b) the two middle regions, and (c) the center region are exposed with a unit dose.

dose distribution types (type-V, type-M, and type-A), but the details are different. The dose distribution is adjusted so that it is guided toward a given type and the maximum of the width errors is minimized.

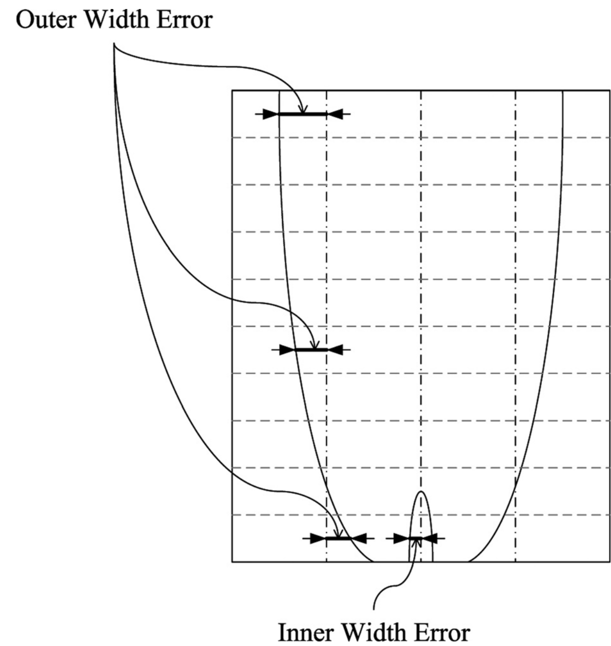

FIG. 9. Outer width errors and the inner width errors defined at the cross-section of the resist profile.

Note that since the base exposures are precalculated, the cost for exposure computation in the first step during iterations can be greatly reduced. Also, the path-based method in the second step saves a lot of simulation time for the resist development process. These improvements make the proposed dose optimization scheme an efficient and effective alternative to the conventional PEC approach (also refer to the flowchart in Fig. 10).

V. RESULTS AND DISCUSSION

The effectiveness of different dose distribution types (type-V, type-M, and type-A) in achieving a vertical sidewall, using the new dose optimization scheme, have been analyzed through simulation. The *PSF*s used in the simulation are generated by a Monte Carlo simulation method, SEEL.[16] The substrate systems employed in the simulation are composed of PMMA on Si where the three different PMMA thicknesses, 100, 300, and 500 nm, are considered. The beam energy is set to 50 keV with a beam diameter of 5 nm. Two different widths of a single-line were considered for performance analysis, i.e., 50 and 100 nm, and the length of the line is fixed at 3 μm. These three substrate systems along with the two feature sizes provide six different combinations so that the proposed scheme can be thoroughly tested. The line features were corrected with the three dose distribution types, i.e. type-V, type-M, and type-A, for a target resist profile of a vertical sidewall. The simulation results for no correction (a uniform dose distribution) and correction using different dose distribution types are compared in terms of the resist profile with the constraint that the total dose, which is $\sum_{i=1}^{5} d(i)$, must be the same for all distribution types.

Downloaded 10 Dec 2012 to 131.204.21.179. Redistribution subject to AVS license or copyright; see http://avspublications.org/jvstb/about/rights_and_permissions

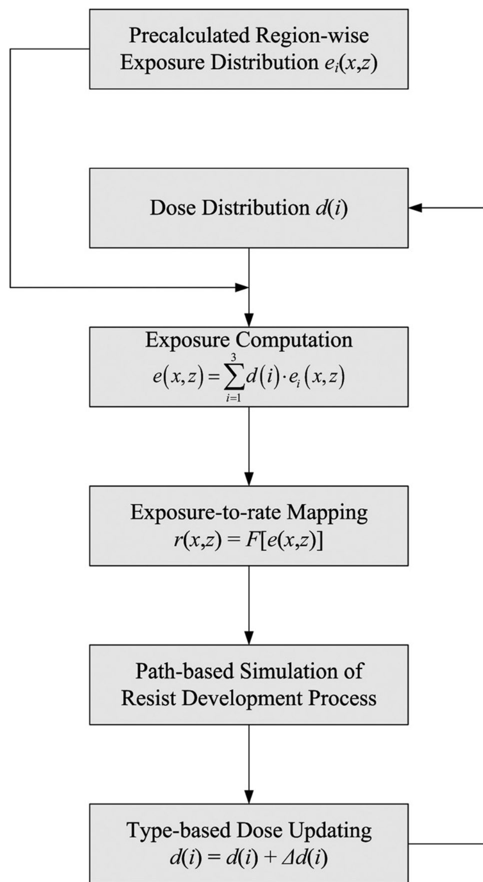

FIG. 10. Flowchart of the proposed dose optimization scheme.

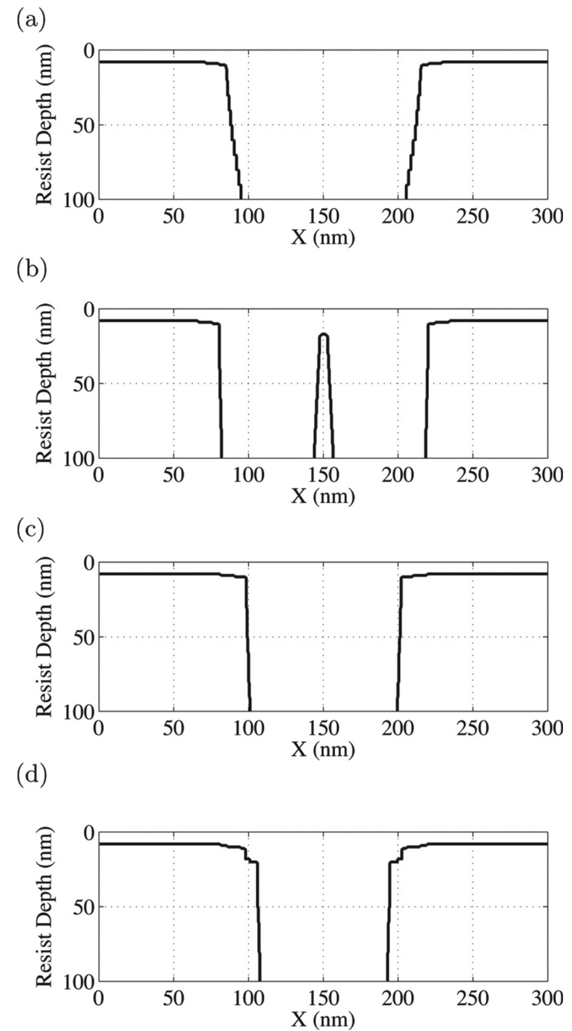

FIG. 11. Cross-section resist profiles: (a) the uniform dose distribution, (b) the type-V dose distribution, (c) the type-M dose distribution, and (d) the type-A dose distribution on the substrate system of 100 nm PMMA on Si (total dose 140 $\mu C/cm^2$).

The results (cross-section resist profiles) are provided in Figs. 11–13. From the profiles obtained by the uniform dose distribution [Figs. 11(a), 12(a), and 13(a)], it can be seen that the resist profile significantly deviates from the target profile of a vertical sidewall. The line width is much greater and the sidewall is clearly overcut. Looking at the resist profiles [Figs. 11(b), 12(b), and 13(b)] obtained by the type-V dose distribution, it can be seen that they are better than those by the uniform dose distribution, but the deviation from the target resist profile is still substantial, and they are even slightly worse than the uniform dose distribution results in a few cases. Also, the resist profiles here are not always fully developed, which indicates that the type-V dose distribution requires a higher total dose. The resist profiles obtained by the type-M [Figs. 11(c), 12(c), and 13(c)] and type-A [Figs. 11(d), 12(d), and 13(d)] dose distributions are much closer to the target profile in terms of line width and sidewall shape.

In Fig. 14, the resist profiles achieved and total doses required by different dose distributions are provided. In this simulation, the lowest total dose needed to achieve a fully developed resist profile as close to the target profile of vertical sidewall as possible is found through enumeration for each dose distribution type. It can be seen that the type-A dose distribution requires the lowest total dose, which is 46.51% less than that of the uniform dose distribution. The type-M dose distribution performs the second best, as achieving a total dose reduction of 41.86% compared to the uniform dose distribution, while the total dose reduction of the type-V dose distribution is only 25.58%.

The correction methods are also compared quantitatively in terms of the percent width errors.

$$\text{Average Percent Width Error} = \frac{1}{n}\sum_{j=1}^{n}\frac{|p(j)-q(j)|}{q(j)} \times 100\%, \tag{7}$$

$$\text{Max Percent Width Error} = \max_{j=1}^{n}\frac{|p(j)-q(j)|}{q(j)} \times 100\%, \tag{8}$$

where $p(j)$ is the width of the j-th layer in the final resist profile after correction, $q(j)$ is the target profile, and n is the number of resist layers (refer to Fig. 3).

The average and maximum percent width errors are provided in Table I. Note that the maximum error reaches 100%

Downloaded 10 Dec 2012 to 131.204.21.179. Redistribution subject to AVS license or copyright; see http://avspublications.org/jvstb/about/rights_and_permissions

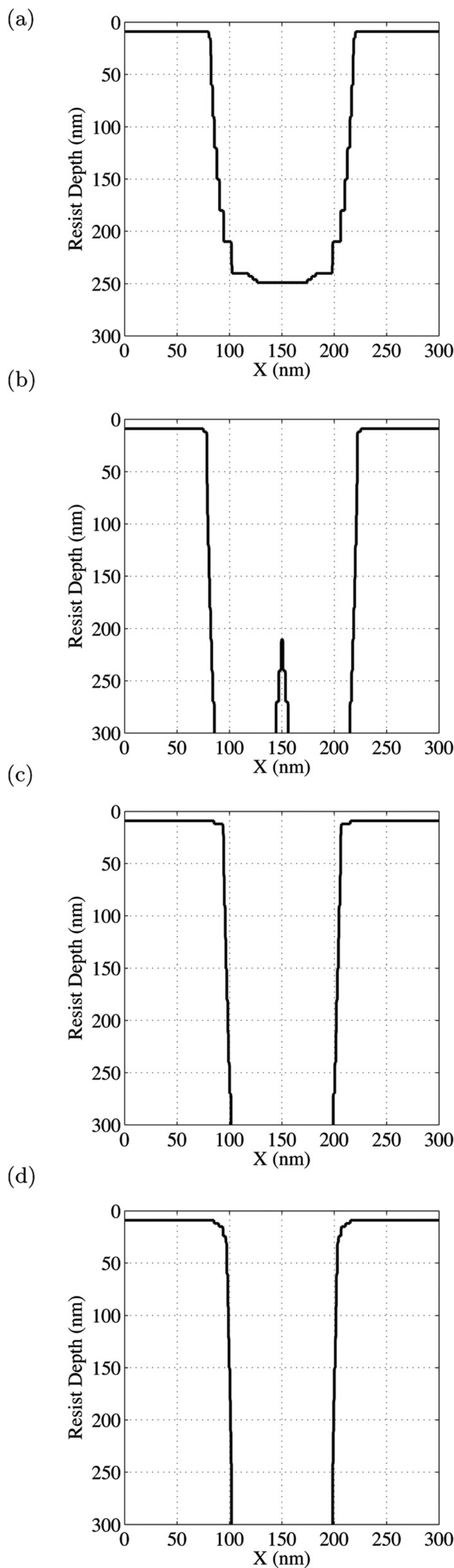

FIG. 12. Cross-section resist profiles: (a) the uniform dose distribution, (b) the type-V dose distribution, (c) the type-M dose distribution, and (d) the type-A dose distribution on the substrate system of 300 nm PMMA on Si (total dose 250 $\mu C/cm^2$).

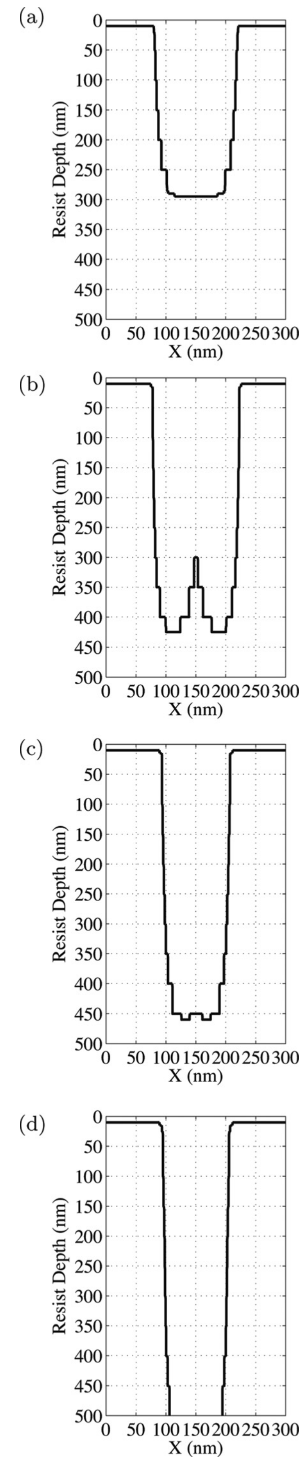

FIG. 13. Cross-section resist profiles: (a) the uniform dose distribution, (b) the type-V dose distribution, (c) the type-M dose distribution, and (d) the type-A dose distribution on the substrate system of 500 nm PMMA on Si (total dose 290 $\mu C/cm^2$).

in some cases, due to the underdevelopment in resist profiles (e.g., the bottom layer is not developed at all, leading to a zero width). The results show that the errors for the type-M and type-A dose distributions are significantly smaller than those for the type-V dose distribution, as both average and maximum errors are greatly reduced.

From Table I, it is observed that the type-M dose distribution has the best result when the ratio of resist thickness to feature size is small, e.g., 1:1. However, as this ratio increases, the type-A dose distribution tends to be the best

Downloaded 10 Dec 2012 to 131.204.21.179. Redistribution subject to AVS license or copyright; see http://avspublications.org/jvstb/about/rights_and_permissions

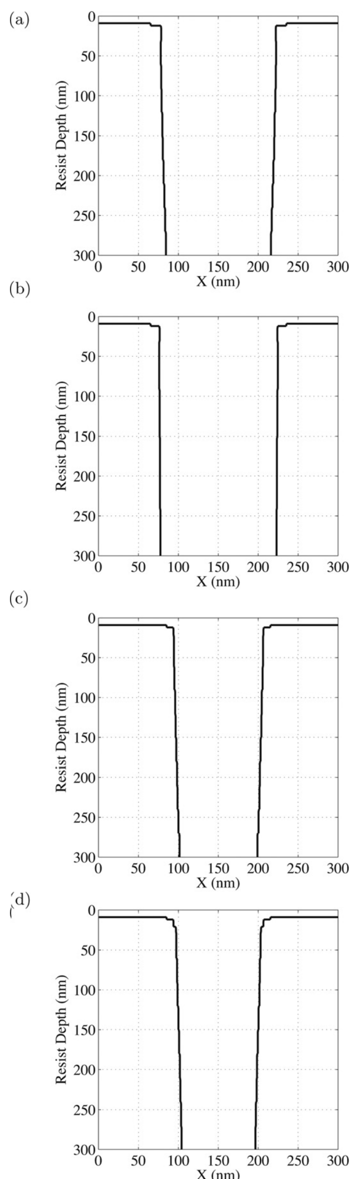

FIG. 14. Cross-section resist profiles: (a) the uniform dose distribution (total dose 430 $\mu C/cm^2$), (b) the type-V dose distribution (total dose 320 $\mu C/cm^2$), (c) the type-M dose distribution (total dose 250 $\mu C/cm^2$), and (d) the type-A dose distribution (total dose 230 $\mu C/cm^2$) on the substrate system of 300 nm PMMA on Si.

one. On one hand, for a thicker resist, the exposure variation along the depth dimension is larger, i.e., the difference of developing rates between the top and the bottom layers becomes larger. On the other hand, for a smaller feature size, the lateral path for the bottom layer of resist to catch up with that of the top layer is shorter. Therefore, it is better to concentrate exposure (equivalently dose) at the center region in order to let the bottom layer develop laterally relatively earlier. Therefore, the type-A dose distribution is more suitable for fabrication of features in an extremely small scale.

VI. SUMMARY

New types of dose distributions, i.e. type-M and type-A, have been derived under our 3-D model and PEC for achieving a target resist profile of a vertical sidewall for nanoscale features with the minimum total dose. The new dose-distribution types take the exposure variation along the resist depth dimension (in addition to the lateral dimensions) into account, and balance vertical and lateral developments of the resist through the resist layers for realization of the target profile. Also, a dose optimization scheme has been developed, which consists of a systematic dose updating procedure coupled with a fast exposure computation and a path-based resist development simulation. This dose optimization scheme is not only fast and effective, but also adaptable to different dose distribution types. Through an extensive simulation, it has been shown that the proposed type-M and type-A dose distributions can significantly improve correction results, when compared to the conventional type-V dose distribution, in terms of achieving the target resist profile, i.e., not only the CD error but also the sidewall shape, and minimizing the total dose. Therefore, the proposed dose-distribution types have a good potential to be employed for fabrication of nanoscale features.

The current and future efforts include verifying the simulation results experimentally, extending the results to patterns of multiple features, and employing the proposed dose distribution types for other sidewall shapes.

TABLE I. Average and maximum percent width errors in resist profiles (among top, middle and bottom layers) for uniform, type-V, type-M and type-A dose distributions.

Simulation Settings		Uniform		Type-V		Type-M		Type-A	
PMMA Thickness	Feature Size	Avg (%)	Max (%)	Avg (%)	Max (%)	Avg (%)	Max (%)	Avg (%)	Max (%)
100 nm	50 nm	64.53	100.00	40.29	70.40	13.78	24.00	5.11	10.00
	100 nm	21.80	30.20	30.97	38.70	2.11	4.00	11.49	14.00
300 nm	50 nm	72.71	100.00	66.53	100.00	39.49	100.00	15.78	28.00
	100 nm	38.06	100.00	36.11	44.00	6.22	12.00	2.67	6.00
500 nm	50 nm	71.69	100.00	78.09	100.00	49.60	100.00	36.22	48.00
	100 nm	58.34	100.00	45.71	100.00	19.04	94.40	6.00	11.00

Downloaded 10 Dec 2012 to 131.204.21.179. Redistribution subject to AVS license or copyright; see http://avspublications.org/jvstb/about/rights_and_permissions

ACKNOWLEDGMENT

This work was supported by a research grant from Samsung Electronics Co., Ltd.

[1]R. Rau, J. McClellan, and T. Drabik, J. Vac. Sci. Technol. B **14**, 2445 (1996).
[2]G. P. Watson, L. A. Fetter, and J. A. Liddle, J. Vac. Sci. Technol. B **15**, 2309 (1997).
[3]G. P. Watson, S. D. Berger, and J. A. Liddle, J. Vac. Sci. Technol. B **16**, 3256 (1998).
[4]S.-Y. Lee and B. D. Cook, IEEE Trans. Semicond. Manuf. **11**, 108 (1998).
[5]C. S. Ea and A. D. Brown, J. Vac. Sci. Technol. B **17**, 323 (1999).
[6]U. Hofmann, R. Crandall, and L. Johnson, J. Vac. Sci. Technol. B **17**, 2940 (1999).
[7]K. Takahashi, M. Osawa, M. Sato, H. Arimoto, K. Ogino, H. Hoshino, and Y. Machida, J. Vac. Sci. Technol. B **18**, 3150 (2000).
[8]C. S. Ea and A. D. Brown, J. Vac. Sci. Technol. B **19**, 1985 (2001).
[9]M. Osawa, K. Takahashi, M. Sato, H. Arimoto, K. Ogino, H. Hoshino, and Y. Machida, J. Vac. Sci. Technol. B **19**, 2483 (2001).
[10]S.-Y. Lee and K. Anbumony, Microelectron. Eng. **83**, 336 (2006).
[11]K. Anbumony and S.-Y. Lee, J. Vac. Sci. Technol. B **24**, 3115 (2006).
[12]S.-Y. Lee and K. Anbumony, J. Vac. Sci. Technol. B **25**, 2008 (2007).
[13]Q. Dai, S.-Y. Lee, S.-H. Lee, B.-G. Kim, and H.-K. Cho, J. Vac. Sci. Technol. B **29**, 06F314 (2011).
[14]Y. Hirai, S. Tomida, K. Ikeda, M. Sasago, M. Endo, S. Hayama, and N. Nomura, IEEE Trans. Comput.-Aided Des. **10**, 802 (1991).
[15]Q. Dai, S.-Y. Lee, S.-H. Lee, B.-G. Kim, and H.-K. Cho, Microelectron. Eng. **88**, 902 (2011).
[16]S. Johnson, "Simulation of electron scattering in complex nanostructures: Lithography, metrology, and characterization," Ph.D. dissertation (Cornell University, Ithaca, NY, 1992).

Downloaded 10 Dec 2012 to 131.204.21.179. Redistribution subject to AVS license or copyright; see http://avspublications.org/jvstb/about/rights_and_permissions